Analysis of Phase Recovery Algorithms for DP-QPSK Optical Receivers

Hugo B. Ferreira, Valery N. Rozental, Darli A. A. Mello

***Abstract*— This paper compares the performance of phase recovery techniques for optical dual-polarization quadrature phase-shift keying (DP-QPSK) coherent receivers, using simulated and experimental data. In particular, we investigate the following phase recovery techniques: the Viterbi & Viterbi feedforward (V&V) algorithm; the decision-directed (DD) algorithm; and a hardware efficient feedforward algorithm.**

We find that 10 tap filters are sufficient for a satisfactory performance of both DD and V&V algorithms, and that the hardware efficient algorithm presents a minimum penalty, compared to the V&V algorithm, for a 5 tap filter size. The problem of obtaining the SNR at the receiver from a set of noise corrupted samples is also addressed.

***Keywords*— dual-polarization quadrature phase-shift keying, phase noise, phase recovery, SNR estimation.**

I. Introduction

The increasing demand for data traffic in optical networks has been motivating the development of spectrally-efficient systems using polarization multiplexing and multilevel modulation formats. DP-QPSK coherent detection systems have emerged as an attractive alternative to meet this demand. These systems require sophisticated signal treatment techniques, done by digital signal processing. One degrading effect that a receiver must compensate is the phase noise of the transmitter and receiver oscillators, modeled by a Wiener process [1]. Several techniques for phase noise compensation, known as phase recovery algorithms, are found in literature [2], [3], [4], [5].

In this paper we simulate and compare the performance of some of these techniques, validating our simulations by experimental data processing. The experimental data was generated by the setup described in [6]. We investigate the Viterbi & Viterbi feedforward phase recovery algorithm (V&V), the decision-directed phase recovery algorithm (DD) [2] and a hardware efficient feedforward phase recovery algorithm [3], using Monte Carlo simulations. Two of these algorithms, V&V and DD, employ a maximum likelihood (ML) estimator, that requires the SNR as a parameter. Thus, an error in the SNR estimation affects the accuracy of the ML estimator, worsening the system performance. We investigate the impact of SNR estimation errors on the system performance.

The rest of the paper is structured as follows: Section II overviews the system model; Section III describes the phase recovery and the SNR estimation algorithms used in this paper; Section IV presents the experimental results; Section V summarizes the results and draws conclusions.

II. System Model

Fig. 1 shows the discrete time system model used in this paper.

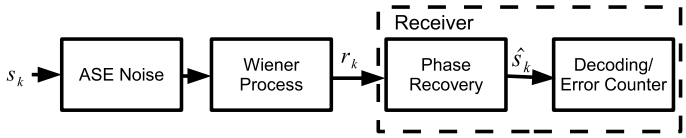

Fig. 1. System model.

The QPSK signal, corrupted by amplified spontaneous emission noise (ASE), modeled as complex additive white Gaussian noise (AWGN) with zero mean and variance $\sigma_w^2 = N_0$, is submitted to a Wiener process that models the phase noise [1]. Two blocks of the receiver structure perform phase recovery, decoding and error counting.

The k-th received complex signal sample, r_k, is given by:

$$r_k = s_k \exp(j\theta_k) + w_k, \tag{1}$$

where s_k is the transmitted symbol, w_k is the complex AWGN sample and θ_k is the phase offset. We model θ_k as a discrete Wiener process by:

$$\begin{aligned} \theta_k &= \theta_{k-1} + \Delta_k, \\ \theta_{k\pm i} &= \theta_k \pm \sum_{m=0}^{i-1} \Delta_m, \end{aligned} \tag{2}$$

where Δ_k and Δ_m are Gaussian distributed random variables with zero mean and variance $\sigma_\Delta^2 = 2\pi\Delta\nu T_s$. Bandwidth $\Delta\nu$ is the sum of the carrier laser and receiver local oscillator (LO) 3 dB linewidths, and T_s is the symbol period. Phase recovery algorithms, therefore, estimate θ_k for the subsequent compensation.

III. Phase Recovery Algorithms

A. Viterbi & Viterbi Feedforward Phase Recovery

The block diagram for the V&V algorithm is shown in Fig. 2.

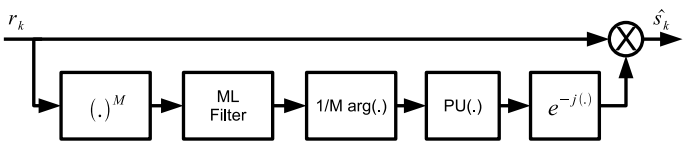

Fig. 2. Viterbi & Viterbi feedforward phase recovery scheme.

Firstly, the V&V algorithm removes data dependency of the sampled sequence by raising it to the M-th power [7]:

$$\begin{aligned} r_{k-i}^{M} &= \left\{ s_{k-i} \exp\left[j(\theta_k + \sum_{m=0}^{i-1} \Delta_m) \right] + w_{k-i} \right\}^{M}, \\ &\approx s_{k-i}^{M} \exp\left[jM(\theta_k + \sum_{m=0}^{i-1} \Delta_m) \right] + z_{k-i}, \end{aligned} \quad (3)$$

where z_{k-i} is a Gaussian random variable with zero mean and variance $\sigma_z^2 = M^2 E_s^{M-1} \sigma_w^2$, and $E_s = |s_k|^2$. Assuming low phase noise we approximate $\exp\left(\sum_{m=0}^{i-1} \Delta_m\right)$ by the first two terms of its Taylor series:

$$r_{k-i}^{M} \approx E_s^{M/2} \exp(jM\theta_k) \left(1 + jM \sum_{m=0}^{i-1} \Delta_m \right) + z_{k-i}.$$

Thus, for a given θ_k, the conditional probability density function (pdf) of a 2N+1 size vector $\mathbf{r}$ of past and future samples, raised to *M*-th power:

$$\mathbf{r} = [r_{k-N}^{M}, ..., r_{k-1}^{M}, r_k^{M}, r_{k+1}^{M}, ..., r_{k+N}^{M}] \quad (4)$$

is given by a multi-variable Gaussian distribution function:

$$\begin{aligned} f_{\mathbf{r}|\theta[k]}(\mathbf{r} \,|\, \theta[k]) &= \frac{1}{(2\pi)^{(2N+1)/2} \, |\mathbf{C}|^{1/2}} \times \quad (5) \\ &\times \exp\left[-\frac{1}{2} (\mathbf{r} - \mathbf{m}_\mathbf{r})^H \, \mathbf{C}^{-1} (\mathbf{r} - \mathbf{m}_\mathbf{r}) \right], \quad (6) \end{aligned}$$

where

$$\mathbf{m}_\mathbf{r} = \mathrm{E}\{\mathbf{r}\} = E_s^2 \, e^{jM\theta[k]} \mathbf{1}. \quad (7)$$

In the previous equation, $\mathbf{1} = [1 \;\; 1 \;\; \ldots \;\; 1]_{(2N+1)}^{T}$, and $\mathbf{C}$ is a covariance matrix:

$$\mathbf{C} = E_s^M M^2 \sigma_\Delta^2 \mathbf{K} + E_s^{M-1} M^2 \sigma_w^2 \mathbf{I}_{(2N+1)\mathrm{x}(2N+1)}, \quad (8)$$

with

$$\mathbf{K} = \begin{bmatrix} N & \cdots & 2 & 1 & 0 & 0 & 0 & \cdots & 0 \\ \vdots & \ddots & \vdots & \vdots & \vdots & \vdots & \vdots & \iddots & \vdots \\ 2 & \cdots & 2 & 1 & 0 & 0 & 0 & \cdots & 0 \\ 1 & \cdots & 1 & 1 & 0 & 0 & 0 & \cdots & 0 \\ 0 & \cdots & 0 & 0 & 0 & 0 & 0 & \cdots & 0 \\ 0 & \cdots & 0 & 0 & 0 & 1 & 1 & \cdots & 1 \\ 0 & \cdots & 0 & 0 & 0 & 1 & 2 & \cdots & 2 \\ \vdots & \iddots & \vdots & \vdots & \vdots & \vdots & \vdots & \ddots & \vdots \\ 0 & \cdots & 0 & 0 & 0 & 1 & 2 & \cdots & N \end{bmatrix}. \quad (9)$$

The logarithmic ML function is defined as:

$$\theta_k^{ML} = \arg\max_{\theta_k} \ln\left(f_{\mathbf{r}|\theta_k}(\mathbf{r} \,|\, \theta_k) \right). \quad (10)$$

It can be shown that

$$\theta_k^{ML} = \frac{1}{M} \arg\left(\mathbf{1}^T \mathbf{C}^{-1} \cdot \mathbf{r} \right). \quad (11)$$

Finally, a phase unwrapping (PU) block is applied, allowing θ_k to vary from $-\infty$ to $+\infty$, instead of being limited between $-\pi/M$ and $+\pi/M$ [2]. Eq. 12 shows the operation performed by the PU algorithm:

$$PU(\cdot) = (\cdot) + \left(\left\lfloor \frac{1}{2} + \frac{\hat{\theta}_{k-1} - (\cdot)}{2\pi/M} \right\rfloor \right) \frac{2\pi}{M}. \quad (12)$$

The estimated phase deviation for the k-th symbol $\hat{\theta}_k$ is, therefore:

$$\hat{\theta}[k] = PU\left\{ \frac{1}{4} \arg\left(\mathbf{1}^T \, \mathbf{C}^{-1} \cdot \mathbf{r} \right) \right\}. \quad (13)$$

We define ML filter as:

$$\mathbf{W} = \mathbf{C}^{-1} \cdot \mathbf{1}^T. \quad (14)$$

The ML filter shape depends on the SNR and the Wiener noise process parameter. Fig. 3 shows the normalized coefficients of a 41 tap ML filter for a fixed $\Delta\nu T_s = 10^{-3}$. We observe that an increase in SNR narrows the filters shape, making it more selective to the phase noise.

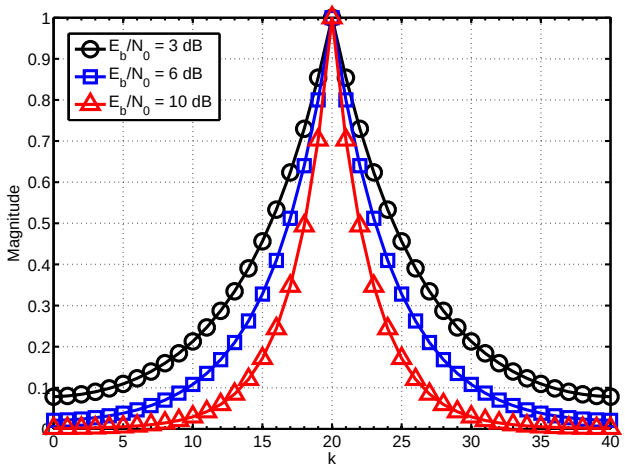

Fig. 3. ML filter coefficients for $\Delta\nu T_s = 10^{-3}$ for past and future samples.

B. Decision-Directed Phase Recovery

The block diagram for the DD algorithm is shown in Fig. 4.

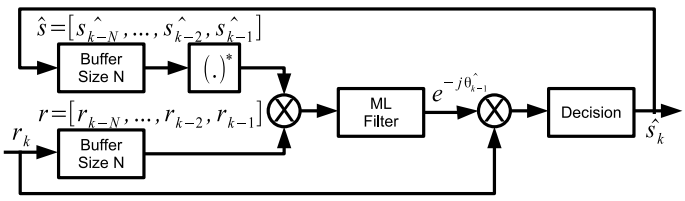

Fig. 4. Decision-directed phase recovery scheme.

The DD algorithm uses N previous output symbols of the minimum distance decision block to remove the data dependency of the input samples [2]. This is accomplished by multiplying the received past samples r_{k-i} by the complex conjugate of the estimated symbols $\hat{s}_{k-i}^{*}$, resulting in the data independent samples $\dot{r}_{k-i}$:

$$\begin{aligned} \dot{r}_{k-i} &= (s_{k-i} e^{j(\theta_k + \sum_{m=0}^{i-1} \Delta_m)} + w_{k-i}) \hat{s}_{k-i}^{*}, \\ &\approx E_s e^{j(\theta_k + \sum_{m=0}^{i-1} \Delta_m)} + \underbrace{w_{k-i} \hat{s}_{k-i}^{*}}_{\dot{w}_{k-i}}, \end{aligned} \quad (15)$$

where $\sigma_{\dot{w}}^2 = E_s\sigma_w^2$.

As in case of V&V, an ML filter is used. However, only the past samples are considered, because of the decision requirement.

The sample vector $\dot{\mathbf{r}} = [\dot{r}_{k-N}, ..., \dot{r}_{k-1}]$ is used as the input for the ML filter **W**, described as:

$$\mathbf{W} = \mathbf{C}^{-1} \cdot \mathbf{1}^T, \tag{16}$$

where the covariance matrix **C** is defined by:

$$\mathbf{C} = E_s^2\sigma_\Delta^2\mathbf{K} + E_s\sigma_w^2\mathbf{I}_{N\text{x}N}, \tag{17}$$

and **K** is an NxN matrix for a filter size of N taps:

$$\mathbf{K} = \begin{bmatrix} 0 & 0 & 0 & \cdots & 0 \\ 0 & 1 & 1 & \cdots & 1 \\ 0 & 1 & 2 & \cdots & 2 \\ \vdots & \vdots & \vdots & \ddots & \vdots \\ 0 & 1 & 2 & \cdots & N-1 \end{bmatrix}. \tag{18}$$

The filter output is the estimated complex phasor $e^{j\hat{\theta}_{k-1}}$ used to compensate for the k-th symbol phase offset. The k-th estimated symbol, $\hat{s}_k$, is then:

$$\hat{s}_k = r_k \left(\sum_{i=1}^{N} \dot{r}_{k-i} W_i \right), \tag{19}$$

where W_i is the i-th coefficient of the ML filter.

The DD ML filter exhibits a similar behavior as those in Fig. 3. However, only the past samples are considered in this case. Since this algorithm relies on decided symbols, erroneous decisions may lead to poor phase estimation. Therefore, it is only accurate for sufficiently high SNRs.

C. SNR Estimation

Implementation of an ML filter requires the signal SNR. We used the scheme proposed in [8] to estimate the symbol energy, E_s, and the noise variance, N_0, of the AWGN process:

$$\hat{E}_s = \sqrt{2\overline{|r|^2}^2 - \overline{|r|^4}}, \tag{20}$$

$$\hat{N}_0 = \overline{|r|^2} - E_s, \tag{21}$$

where r is the received signal. In this work, the SNR estimation was performed over a set of 5×10^5 symbols.

D. Hardware Efficient Feedforward Recovery

The V&V and the DD algorithms involve high complexity operations, such as complex multiplications, feedback scheme and serial processing, inefficient for hardware implementation in high rate real-time systems.

One alternative is a multiplier-free angle-based algorithm, proposed in [3]. This algorithm, whose block diagram is shown in Fig. 5, in addition to dispensing complex multiplications, does not require feedback and allows parallel processing.

The phase deviation term, ϑ_k, is calculated by the following operation:

$$\vartheta_k = 1/4(arg(r_k^4)). \tag{22}$$

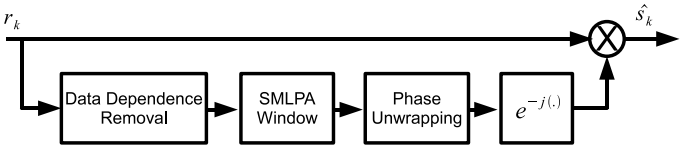

Fig. 5. Hardware efficient phase recovery scheme.

The estimation process is based on a sliding window with $2N+1$ inputs for each estimated $\hat{\theta}$, or $2N+M$ for an M size block output, performing selective operations to approximate the ML filter. The window uses intermediate cells multiple times in parallel, increasing computational efficiency. This process is named SMLPA (selective maximum likelihood phase approximation) [3].

In this paper we use the SLMPA algorithm for $M = 4$ and $N = 2$ (SML2), shown in Fig. 6, with the basic cell operation defined as:

$$\mu = 1/4(arg(e^{j4\alpha} + e^{j4\beta})), \tag{23}$$

where α and β are the cell inputs and μ is the sell output.

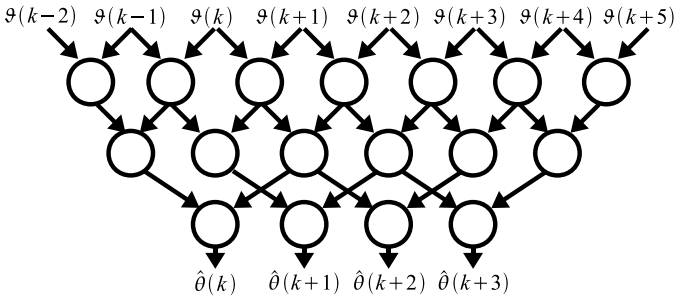

Fig. 6. Sliding window scheme for $N = 2$ and $M = 4$.

Each output, $\hat{\theta}(k+i)$, is computed by submitting the samples $\vartheta(k+i)$, $\vartheta(k+i\pm1)$ and $\vartheta(k+i\pm2)$ to the mesh of the basic cell operations. Nevertheless, the sample weight distribution is unequal, with the sample $\vartheta(k+i)$ being the most significant, and $\vartheta(k+i\pm2)$, the least significant ones. Grafically (see Fig. 6), this weight distribution is represented by the number of cells in the path from each sample to the corresponding output. The structure can be modeled by a pyramid-like filter, with the highest peak value at the middle, decreasing in discreet steps to both sides.

IV. Simulation and Experimental Results

This section starts with the analysis of the impact of imperfect SNR estimation on the system performance. For that purpose, we forced SNR estimation errors in the V&V algorithm, while observing the BER penalization. Figs. 7 and 8 show SNR versus BER curves for rates of 10 Gbaud and 25 Gbaud and 1 MHz laser linewidth, resulting in $\Delta\nu T_s = 2.0 \times 10^{-4}$ and $\Delta\nu T_s = 8.0 \times 10^{-5}$, respectively.

The figures also show the theoretical limit curve for differential coherent QPSK (DCQPSK) systems that is given by [9]:

$$BER = \textbf{erfc}\left(\sqrt{\frac{E_b}{N_0}}\right),$$

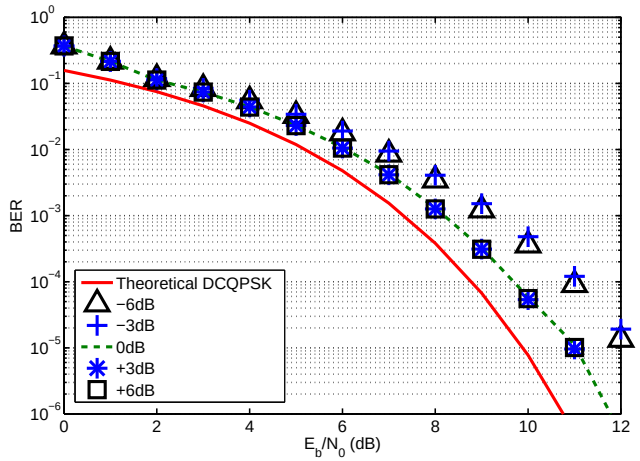

Fig. 7. Eb/N0 x BER curves for 10 Gbaud, 1 MHz lasers and 41 taps V&V.

where **erfc** is the complementary error function.

Since the SNR defines the optimal shape of the ML filter, its erroneous estimation causes performance penalties. SNR underestimation broadens the filter, making distant samples more significant, reducing filter phase noise selectivity. On the other hand, SNR overestimation narrows the filter, increasing phase noise selectivity, but penalizing additive noise mitigation. Fig. 7 shows, however, that the degradation in the last case is less severe, because the narrowed filter is still sufficiently large and robust for additive noise effects. For the 41 taps ML filter used, SNR estimation errors up to +6 dB are insignificant to the phase estimation, while errors of -3 dB and -6 dB degrade the performance significantly.

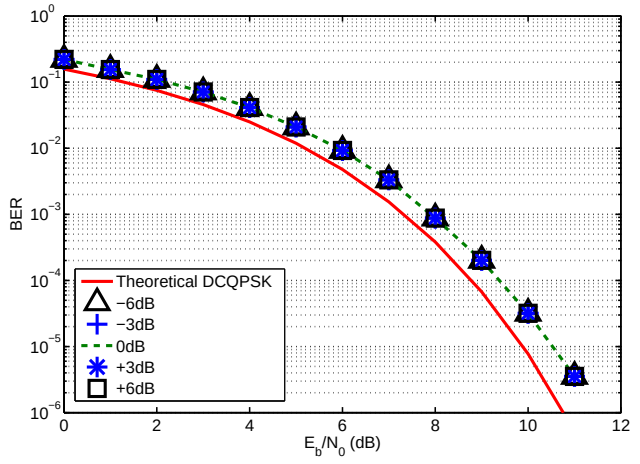

Fig. 8. Eb/N0 x BER curves for 25 Gbaud, 1 MHz lasers and 41 taps V&V.

For the baud rate of 25 Gbaud, the V&V algorithm with 41 taps ML filter does not show penalties for the SNR estimation errors from -6 dB to +6 dB (see Fig. 8). Shorter symbol period makes the phase noise less significant and the estimation more tolerant to changes of the ML filter shape.

We also simulated systems that employ the V&V, the DD and the SMLPA phase recovery algorithms, varying the filter lengths and comparing their performances in terms of phase noise tolerance. A computer simulated input sequence of 4×10^6 bits was used in each case. In Figs. 9 and 10 we plotted penalty curves for a fixed BER of 10^{-3}, restricting the phase noise conditions and observing the SNR penalties.

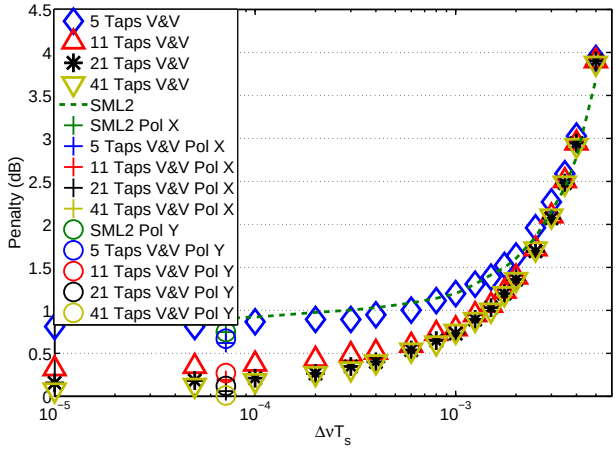

Fig. 9. Filter length effect for V&V and SML2 algorithms.

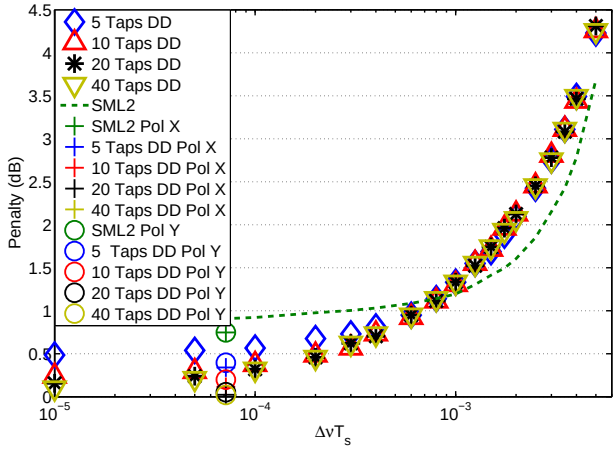

Fig. 10. Filter length effect for DD and SML2 algorithms.

We observe that the increment in the filter length improves both the V&V and the DD algorithms performance only for low phase noise conditions. For a higher phase noise, larger filter increases the complexity without improving the performance. A 5 tap case of SMLPA is also shown for comparison.

In a 5 tap case, for $\Delta\nu T_s$ smaller than 3×10^{-4}, all algorithms show penalties smaller than 1 dB, with a good approximation of the feedforward filter by the SMLPA, that presents almost equal performance for any tested $\Delta\nu T_s$. The DD algorithm shows a slightly better performance for $\Delta\nu T_s$ values smaller than 8×10^{-4}. With increased phase noise their performances rapidly degrade.

Considering the best case scenario (41 taps V&V, 40 taps DD, 5 taps SMLPA), in the low phase noise region, the V&V and the DD achieve a similar, close to the theoretical limit performance, while SMLPA shows a penalty of almost 1 dB. Clearly, the filter size is of a great importance in that region. However, because of the erroneous decisions and because the

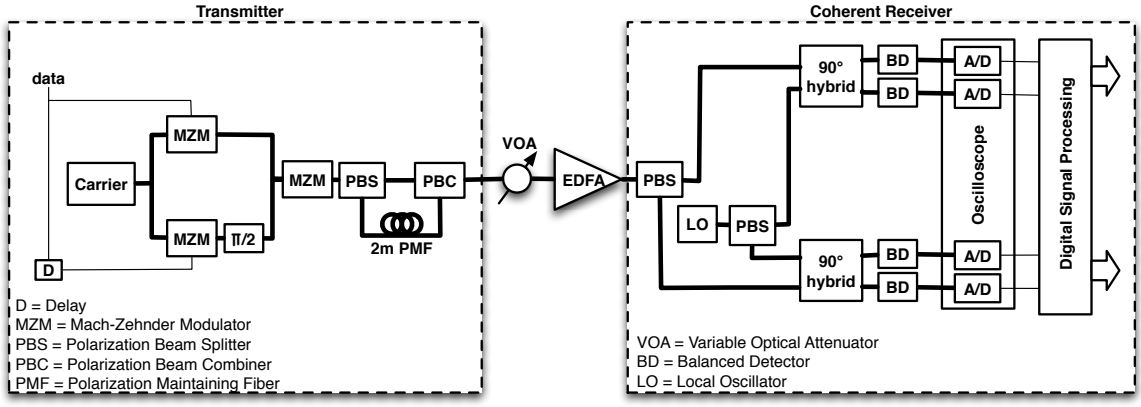

Fig. 11. DP-QPSK experimental setup.

DD filter employs only the past signal samples, in the high phase noise region it is the least successful.

We validated the simulations using experimental data generated by the setup shown in Fig. 11 [6]. At the transmitter, a pseudorandom binary sequence (PRBS) is generated at 28 Gb/s. The original sequence drives the in-phase component of an I/Q Mach-Zehnder modulator (nested structure), while a 51-bits delayed version drives the quadrature component. The resulting optical signal is subsequently RZ-modulated by a pulse carver. Lastly, the polarization multiplexed signal is generated by splitting the optical signal into two orthogonal polarization orientations (using a polarization beam splitter), decorrelating the horizontal (X polarization) and the vertical (Y polarization) components by a 2 meters polarization maintaining fiber, and recombining the two components in a polarization beam combiner. In this experiment 1 MHz linewidth transmitter and local oscillator lasers were used.

In Figs. 9 and 10 "$+$" and "$\circ$" symbols correspond to the penalties calculated over 10^6 bit sequences for X and Y polarizations, respectively. The experimental analysis exhibited a good agreement with the simulations. However, it is observed that the experimentally calculated SNR penalties are slightly lower than the simulated points. This may be because the experimental SNR cannot be directly measured, and has to be estimated from noisy samples. In our case, we believe that the experimental SNR was underestimated.

V. Conclusion

We analyzed the performance of three phase recovery algorithms, along with the impact of SNR estimation on the overall system performance, using computer simulated data. Our analysis showed that even large SNR estimation errors of ± 6 dB lead to no significant penalty for a 100 Gb/s DP-QPSK system with distributed feedback lasers of 1 MHz linewidth. However, for a 40 Gb/s system, in the worst case, 1 dB penalty occurs for a given BER of 10^{-3}. The simulations also showed that both, DD and V&V algorithms with 10 tap filters, have a satisfactory performance, and that a further increment in filter size does not present noteworthy improvements. The SMLPA has shown a good approximation to the V&V for the same filter length. However, to match the performance of the V&V best case scenario, the complexity of SMLPA would have to be increased by adding taps. Therefore, there is a trade off relation between the computational advantage and the performance when choosing the algorithm. We have also shown that the simulated scenarios offer a good representation of practical systems, by direct comparison with experimental data.

VI. Acknowledgment

This work has been supported by Ericsson.

Referências

[1] J. Salz, "Modulation and detection for coherent lightwave communications," *Communications Magazine, IEEE*, vol. 24, no. 6, pp. 38 – 49, jun. 1986.

[2] E. Ip and J. M. Kahn, "Feedforward carrier recovery for coherent optical communications," *J. Lightwave Technol.*, vol. 25, no. 9, pp. 2675–2692, 2007. [Online]. Available: http://jlt.osa.org/abstract.cfm?URI=JLT-25-9-2675

[3] S. Hoffmann, R. Peveling, T. Pfau, O. Adamczyk, R. Eickhoff, and R. Noe, "Multiplier-free real-time phase tracking for coherent QPSK receivers," *Photonics Technology Letters, IEEE*, vol. 21, no. 3, pp. 137 –139, feb.1, 2009.

[4] S. Hoffmann, S. Bhandare, T. Pfau, O. Adamczyk, C. Wordehoff, R. Peveling, M. Porrmann, and R. Noe, "Frequency and phase estimation for coherent QPSK transmission with unlocked DFB lasers," *Photonics Technology Letters, IEEE*, vol. 20, no. 18, pp. 1569 –1571, sept.15, 2008.

[5] F. A. Garcia, D. A. Mello, and H. Waldman, "Feedforward carrier recovery for polarization demultiplexed signals with unequal signal to noise ratios," *Opt. Express*, vol. 17, no. 10, pp. 7958–7969, 2009. [Online]. Available: http://www.opticsexpress.org/abstract.cfm?URI=oe-17-10-7958

[6] T. Portela, D. Souto, V. Rozental, H. Ferreira, H. Griesser, and D. Mello, "Analysis of digital polarization demultiplexing techniques for optical 112 Gb/s DP-QPSK receivers with experimental data," *Journal of Microwaves, Optoelectronics and Electromagnetic Applications (JMOe)*, vol. 10-1, pp. 155–164, 2011.

[7] A. Viterbi, "Nonlinear estimation of PSK-modulated carrier phase with application to burst digital transmission," *Information Theory, IEEE Transactions on*, vol. 29, no. 4, pp. 543–551, 1983. [Online]. Available: http://ieeexplore.ieee.org/xpls/abs_all.jsp?arnumber=1056713

[8] T. Benedict and T. Soong, "The joint estimation of signal and noise from the sum envelope," *Information Theory, IEEE Transactions on*, vol. 13, no. 3, pp. 447 – 454, jul 1967.

[9] S. Haykin, *Communication Systems*, 4th ed. USA: Wiley, 2001.